Journal of Applied Polymer Science

Foaming Behavior of Microcellular Foam Polypropylene/Modified Nano Calcium Carbonate Composites

Jie Ding, Junnan Shangguan, Weihua Ma, Qin Zhong
College of Chemical Engineering, Nanjing University of Science and Technology, Nanjing, Jiangsu 210094, People's Republic of China
Correspondence to: W. H. Ma (E-mail: maweihuacn@yahoo.com.cn) or Q. Zhong (E-mail: zq304@mail.njust.edu.cn)

ABSTRACT: A new process was used to prepare microcellular foams with supercritical carbon dioxide as the physical foaming agent in a batch. The foaming temperature range of the new process was about five times broader than that of the conventional one. Characterization of the cellular structure of the original polypropylene (PP) and PP/nano-$CaCO_3$ (nanocomposites) foams was conducted to reveal the effects of the blend composition and processing conditions. The results show that the cellular structure of the PP foams was more sensitive to the foaming temperature and saturation pressure variations than that of the nanocomposite foams. Uniform cells of PP foams are achieved only at a temperature of 154°C. Also, the low pressure of 20 MPa led to very small cells and a low cell density. The competition between the cell growth and cell nucleation played important role in the foam density and was directly related to the foaming temperature. Decreasing the infiltration temperature depressed the initial foaming temperature, and this resulted in significantly larger cells and a lower cell density. A short foaming time led to a skin–core structure; this indicated that a decrease in the cell size was found from skin to core, but the skin–core structure gradually disappeared with increasing foaming time.
 J. Appl. Polym. Sci. 128: 3639–3651, 2013

KEYWORDS: foaming; microcellular; nano calcium carbonate; polypropylene; SC-CO_2

Received 20 March 2012; accepted 28 July 2012; published online 8 October 2012
DOI: 10.1002/app.38416

INTRODUCTION

Polymer microcellular foams usually refer to foams with an average cell diameter smaller than 10 μm and a cell density higher than 10^9 cells/cm^3.[1,2] Because of its ultrasmall cell size and high cell density, the microcellular foams have a light weight and can provide a higher mechanical strength and better thermal insulation and acoustic properties compared to conventional polymer foams. Therefore, they are widely used as building materials, auto parts, thermal insulation materials, and so on.

However, microcellular foams are very sensitive to cell size and cell density. It is very difficult to obtain microcellular foams through the foaming of pure polymer, especially a semicrystalline polymer such as polypropylene (PP), because of its low melt strength and inherently poor cell nucleation behavior.[3–5] This is why the foaming of polymers with modifiers has attracted a lot of attention, and nanoparticles are effective modifiers because of their very small sizes and large surface area.[6–9]

On the basis of the route of the induction of thermodynamic instability and the initiation of the foaming process, the application of supercritical carbon dioxide (SC-CO_2) in producing polymeric foams can be classified as temperature-induced or pressure-induced phase separation. Both methods have many disadvantages. In temperature-induced phase separation, the samples must be put into high-temperature oil, and the surface of the sample melts quickly while the interior of the sample remains intact. This leads to nonuniform cells in the foams. In pressure-induced phase separation, the samples are first saturated at temperatures ranging from the glassy temperature to the melting temperature (T_m); this range is very narrow for PP.[3] PP melts easily during saturation, and this reduces its foamability. Huang and Wang[6] combined these two methods and created a new process for foaming polymers. With this new process, PP is saturated at a low temperature, and then, the temperature is increased to the foaming temperature. PP cannot melt easily, and smaller cells and a higher cell density are achieved.

In this study, we systematically examined this new process and proposed two new concepts: *infiltration temperature* (the temperature at which CO_2 dissolves in a rubbery-state polymer),[10,11] and *foaming time* (the polymer softening time). Many previous articles have proposed that only a little CO_2 dissolves in the PP in the rubbery state,[10,11] so the temperature only has a slight effect on cell morphology. However, to our surprise, this study showed that the infiltration temperature had a

Applied Polymer SCIENCE

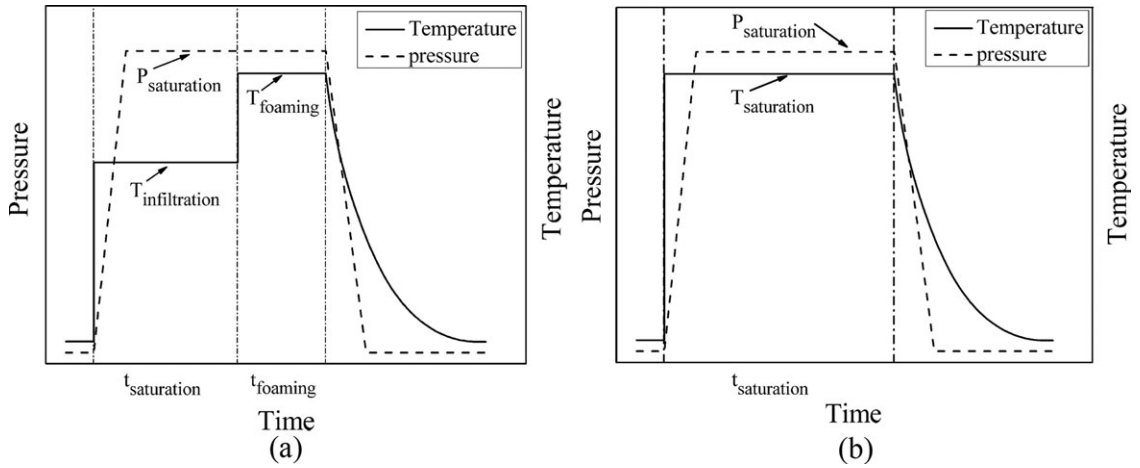

Figure 1. Schematic diagram of the pressure and temperature evolution versus the time in the foaming strategy. The processes were (a) the new process and (b) the conventional process. $P_{saturation}$ is the saturation pressure, $T_{infiltration}$ is the infiltration temperature, $T_{foaming}$ is the foaming temperature, $t_{saturation}$ is the saturetion time, $t_{foaming}$ is the foaming time.

significant effect on the morphology. The foaming time, different from the cell growth time as other articles have proposed,[3,12,13] made a lot of difference in the cell morphology between the surface and interior of PP. Next, we explored the process conditions suitable for obtaining uniform microcells in PP foams. Finally, we compared the new process with the conventional one. Polypropylene/nano-Calcium Carbobnate (PP/nano-$CaCO_3$) nanocomposites were prepared with the melt-blending method with a twin-screw extruder (Nanjing, China). Then, the nanocomposites were used to prepare foams by a batch process in a pressure vessel with SC-CO_2 as a blowing agent.

EXPERIMENTAL

Materials

The PP used was F401 (Sinopec Yangzi Petrochemical Co., Ltd., Sinopec, China) with a melt index of 2.3 g/10 min at 230°C. This PP was injection grade. Nano-$CaCO_3$, with an average diameter of 80–120 nm, was provided by Nanjing Guanye Chemical Co., Ltd. (Nanjing, China). The silane coupling agent (KH550) was purchased from Nanjing Xiangqian Chemical Co., Ltd. (Nanjing, China). Industrial CO_2, purchased from Nanjing Gas Company of 55th Institute (Nanjing, China) with a purity of 99%, was used directly as a foaming agent.

Preparation of Nanocomposites

As previously reported,[14–16] surface modification can improve the adhesion between nanoparticles and a polymer and inhibit nanoparticle aggregation. In this study, we used a silane coupling agent (KH550) to modify the surface of nano-$CaCO_3$. The procedures were as follows: the nano-$CaCO_3$ was dried under vacuum at 60°C for 8 h and then mixed with the coupling agent for 2 h in ethanol. The concentration of the coupling agent was 2 wt % with respect to the nano-$CaCO_3$. The modified nano-$CaCO_3$ was dried again at 60°C until it reached a constant weight.

The PP and nano-$CaCO_3$ were dry-mixed thoroughly and then fed into a twin-screw extruder with a screw diameter of 35.6 mm and a length-to-diameter ratio of 40:1. The compounding was carried out with a temperature profile of 175–180–185–185–180–175°C from the hopper to the strand die. The screw speed was set to 150 rpm. The weight percentages of nano-$CaCO_3$ were 3, 5, 7, and 10 wt % (with respect to PP). The extruded strands, with a diameter of about 2–3 mm, were cooled in a water bath and collected.

Foaming Apparatus and Procedures

In this study, the PP and its nanocomposites were foamed with a batch microcellular foaming apparatus, as shown in a previous report.[6] The foaming procedures were as follows:

1. Samples were placed in a high-pressure vessel (internal volume = 500 cm^3) that was calibrated with distilled water by a syringe pump
2. The vessel was slowly flushed with low-pressure CO_2 gas
3. The vessel was heated to the infiltration temperature within 20 min
4. The vessel was pressurized to the saturation pressure with high-pressure CO_2
5. The samples were saturated in the vessel for 24 h at the saturation pressure.
6. The vessel was heated to the foaming temperature within 20 min, with the saturation pressure remaining unchanged during the temperature increase and the temperature was kept the same for some time (foaming time).
7. The vessel was depressurized to atmospheric pressure in less than 10 s.
8. The foamed samples were injected out of the vessel and cooled to the room temperature in the air.

The whole procedure is shown in Figure 1(a).

Characterization

The original and modified nano-$CaCO_3$ were characterized by X-ray diffraction (XRD) with a Bruker D8 Advance diffractometer (Purkinje General Instrument Co., Ltd., China) with Cu Kα radiation (35 kV, 20 mA) in the 2θ interval from 10 to 60°. The samples were prepared by the molding of the powders into small compact plates at ambient temperature. PP and its

nanocomposites were also characterized by XRD. We prepared the samples by pressing the granular PP and nanocomposites into small compact plates at 190°C.

The coupling agent and original and modified nano-$CaCO_3$ were characterized by Fourier transform infrared (FTIR) spectroscopy (recorded on an IS10 FTIR spectrometer, Nicolet, USA) to confirm the existence of the surface-modifying layer on the nano-$CaCO_3$.

An LEO1530VP scanning electron microscope (LEO, Germany) at an acceleration voltage of 15 kV was used to characterize the distribution of the nano-$CaCO_3$ particles. The sample was cryogenically fractured perpendicular to the flow direction after it was immersed in liquid nitrogen for 0.5 h, and the fractured surface was then coated with a thin layer of gold before scanning electron microcopy (SEM) characterization.

Differential scanning calorimetry (DSC) was conducted on PP and its nanocomposites to determine crystallinity with a Mettler–Toledo DSC 823 E (Switzerland). Weighted samples were sealed in aluminum hermetic pans and heated up to 220°C at a rate of 20°C/min to determine the heat of fusion. All measurements were carried out under a nitrogen atmosphere.

The foamed samples were immersed in liquid nitrogen for 30 min and then fractured. The fractured surfaces were coated with gold and then examined with a JSM 6380 SEM instrument (Japan) at an acceleration voltage of 30 kV to observe the cellular structures of the foamed samples. The average cell diameter was obtained by the software Image Proplus (Image Proplus 6.0, America). The number-average diameter (D) of all of the cells in the micrograph was calculated with the following equation:[3]

$$D = \frac{\sum_{i=1}^{n} d_i}{n} \quad (1)$$

where n is the number of cells in the micrograph and d_i is the perimeter-equivalent diameter.

The cell density (N_c) and the expansion ratio (R_V) in the foam were calculated on the basis of eqs. (2)[17] and (3),[3] in which ρ_f (g/cm^3) is the foam density and ρ_p (g/cm^3) is the density of the PP and its nanocomposites. Both were measured according to ASTMD 792-00:

$$N_c = 10^{12} \times \frac{6[1 - \frac{\rho_f}{\rho_p}]}{\pi D^3} \ (\text{cells/cm}^3) \quad (2)$$

$$R_V = \frac{\rho_p}{\rho_f} \quad (3)$$

RESULTS AND DISCUSSION

Characterization of Nano-$CaCO_3$

The XRD patterns of the original and modified nano-$CaCO_3$ are shown in Figure 2. The crystal phase of the original and the modified nano-$CaCO_3$ could be indexed as trigonal in structure.[18] The main characteristic planes (012), (104), (110), (113), (202), (018), (116), and (122), corresponding to 2θ values of 23.2, 29.5, 36, 39.3, 43, 47.5, 48.4, and 57.3°, respectively, were unambiguously assigned to the calcite structure.[19] The pattern

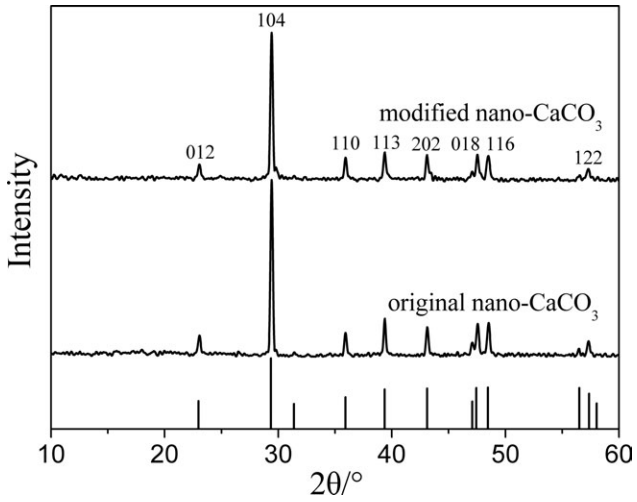

Figure 2. XRD patterns of the original and modified nano-$CaCO_3$ (vertical lines indicate PDF #05-0586).

of the modified nano-$CaCO_3$ did not exhibit any characteristic diffraction peak for the coupling agent, and the intensity of the strongest diffraction (at $2\theta = 29.5°$) was weaker than that of the original nano-$CaCO_3$ (Figure 2); this demonstrated that the coating of the coupling agent on the nano-$CaCO_3$ surface succeeded. The decrease in intensity could have been due to the increase in crystal defects that happened among the crystal particles.[19] The nano-$CaCO_3$ average diameter was quantitatively evaluated from the XRD broadening with the Debye–Scherrer equation.[9] The equation is as follows:

$$D = \frac{K\lambda}{B\cos\theta}$$

where D is the average diameter of the nanoparticles (nm), K is the Scherrer constant ($K = = 0.89$), B is the full width at half-maximum (rad), θ is the diffraction angle (°), and λ is the wavelength of the X-ray (nm; $\lambda = 0.15406$ nm in this study). According to XRD of the original and modified nano-$CaCO_3$, the main diffraction peaks of the original and modified nano-$CaCO_3$ appeared at 2θ values of 29.44 and 29.42°, and the corresponding B values were 1.39×10^{-3} and 1.33×10^{-3} rad, respectively. The average diameters of the original and modified nano-$CaCO_3$ were estimated to be 102 and 107 nm, respectively.

Figure 3 shows the FTIR spectra of the coupling agent and the original and modified nano-$CaCO_3$. The IR spectrum of the original nano-$CaCO_3$ showed three strong peaks at 1459, 872, and 712 cm^{-1}; these peaks corresponded to the antisymmetric stretching, in-plane bending, and plane bending vibrations of CO_3^{2-}, respectively. The broad and weak vibrations at 3448 cm^{-1} were assigned to O—H stretching.[14,20] The peaks at 1102 and 1027 cm^{-1}, corresponding to the stretching vibrations of C—N and Si—O, respectively, appeared in the modified nano-$CaCO_3$ spectrum, but the stretching and bending vibrations of CH_3— at 2950 and about 1500 cm^{-1} (as shown in the circles in Figure 3) and the stretching vibrations of C—O at 1339 cm^{-1} were not found in the spectrum of the modified nano-$CaCO_3$.

Applied Polymer SCIENCE

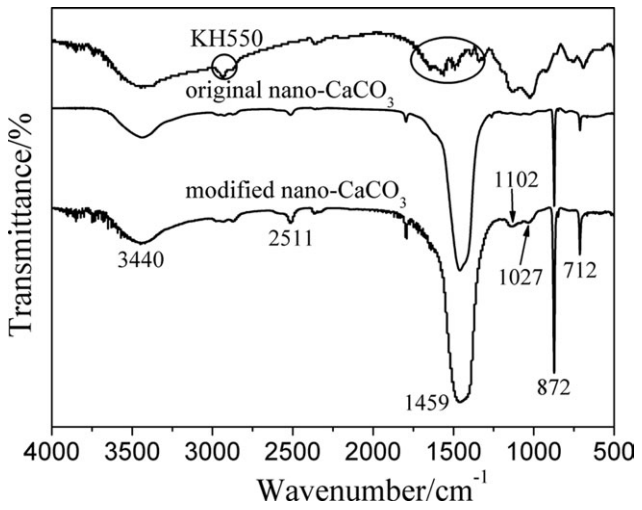

Figure 3. FTIR spectra of the original nano-$CaCO_3$, modified nano-$CaCO_3$, and coupling agent.

This indicated that the O—H groups on the surface of $CaCO_3$ reacted with the coupling agent, and CH_3CH_2O—Si— was substituted by A—O—Si—, where A is the surface of $CaCO_3$, so we could not find the vibrations of CH_3— and C—O. The peak at 3440 cm^{-1} did not disappear for the modified $CaCO_3$ because of the stretching of N—H of the coupling agent. Above all, this indicated covalent bonding instead of physical absorption between the coupling agent and the nano-$CaCO_3$.

Dispersion of Nano-$CaCO_3$ in the PP Matrix

It has been widely accepted that the distribution of nano-$CaCO_3$ is one of the most important factors in determining the foamability of PP,[6] especially for the use of nano-$CaCO_3$ because of its large specific surface area and high surface energy.[21] The more homogeneous the distribution of nano-$CaCO_3$ is, the better the foamability of the nanocomposites will be. Figure 4 shows the distribution of nano-$CaCO_3$ in PP/5% nano-$CaCO_3$ and PP/10% nano-$CaCO_3$ nanocomposites. In the former nanocomposites, nano-$CaCO_3$ tended to disperse singly in the matrix. However, in the latter nanocomposites, nano-$CaCO_3$ tended to form large aggregates with 500–700 nm in size, with aggregations of about 5–7 nano-$CaCO_3$ particles. In other words, a more homogeneous distribution of nano-$CaCO_3$ was achieved in the PP/5% nano-$CaCO_3$ nanocomposites.

Morphology and Properties of PP/Nano-$CaCO_3$

Figure 5 shows the XRD patterns of PP and its nanocomposites. We recall that PP is mainly present in two crystalline forms: α and β.[21,22] For PP, the presence of the α form is revealed by peaks at 14.1, 16.9, 18.5, 21.1, and 21.9°, corresponding to the (110), (040), (130), (111), and (131) planes, respectively. The presence of the β form is revealed by the intense peak at 16.0°, which corresponds to the (300) plane. For the nanocomposites, the intensity of the β-crystalline-phase peak was largely reduced; this showed that nanocomposites had much less β-crystalline-phase polypropylene (β-PP). The decrease of β-PP was attributed to β,α-recrystallization during the melt-blending process; this indicated that β-PP was converted into α-PP. Lei et al.[23] reported that the melting process of β-PP was comprised of three stages: the melting of β-PP, β,α-recrystallization, and the melting of recrystallized α-PP. The relative amount of the β-phase (K value) was determined with the following relation:[24]

$$K = \frac{I_\beta}{I_{\alpha 1} + I_{\alpha 2} + I_{\alpha 3} + I_\beta} \quad (4)$$

where I_β is the intensity of the peak for the (300) diffracting plane of the β phase and $I_{\alpha 1}$, $I_{\alpha 2}$, and $I_{\alpha 3}$ are the intensities of the (110), (040), and (130) planes of the α-phase, respectively. On the basis of eq. (4), the content of β-PP in the PP was about 24%, and those of the nanocomposites were all less than 8%. The peak at 29.0° in the XRD patterns of nanocomposites was the nano-$CaCO_3$. As the content of nano-$CaCO_3$ increased, the intensity of the nano-$CaCO_3$ peak increased apparently.

Melting Behavior of the Nanocomposites

The DSC thermograms of the melting process for PP and its nanocomposites at a heating rate of 20°C/min are shown in Figure 6. For PP/3% nano-$CaCO_3$ and PP/10% nano-$CaCO_3$ nanocomposites, a single melting peak was observed, but the PP, PP/5%nano-$CaCO_3$, and PP/7% nano-$CaCO_3$ had a small melting

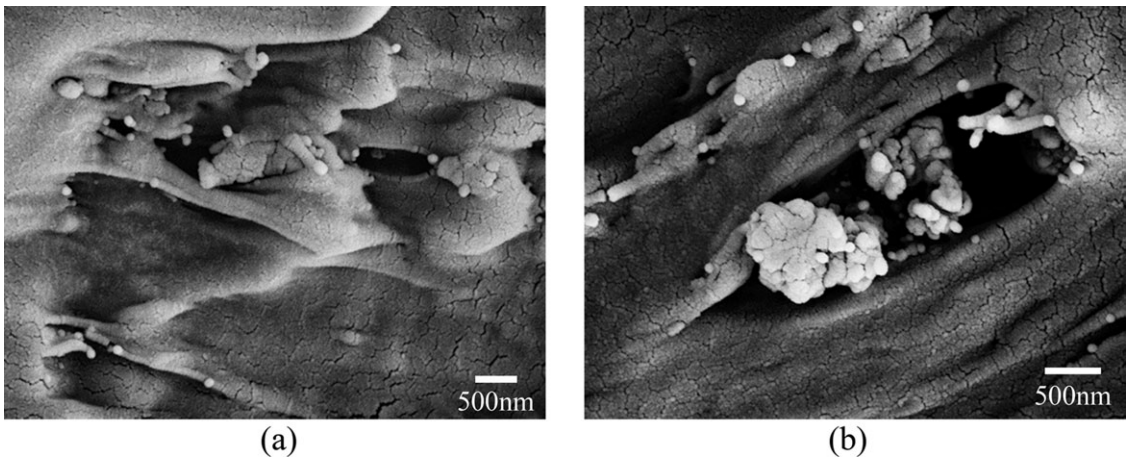

Figure 4. SEM images showing the distribution of nano-$CaCO_3$ in (a) PP/5% nano-$CaCO_3$ and (b) PP/10% nano-$CaCO_3$.

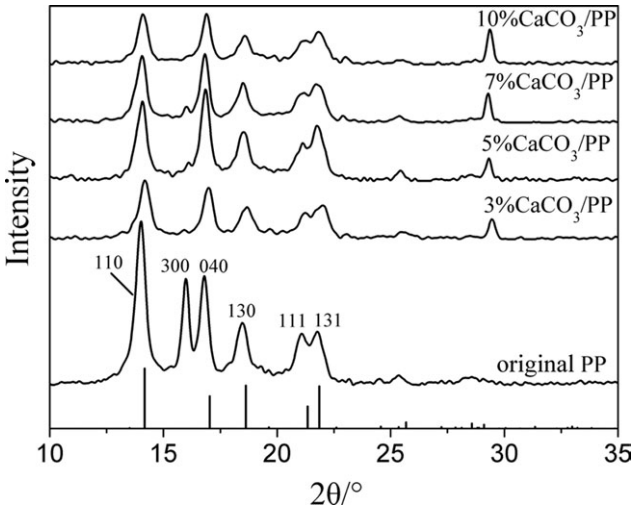

Figure 5. XRD patterns of the original PP and PP/nano-$CaCO_3$ composites (the vertical lines indicate PDF #50-2397).

peak at about 150°C in the low-temperature region of the main melting peak. We attributed this small peak to the melting of β-PP. From Figure 5, we observed the β-crystalline-phase peak in the PP, PP/5% nano-$CaCO_3$, and PP/7% nano-$CaCO_3$, corresponding to their melting behavior in DSC thermograms. However, in PP/3% nano-$CaCO_3$ and PP/10% nano-$CaCO_3$, the same peak was not found. Many previous researchers also found a similar small peak; they all attributed it to the melting of β-PP.[25,26]

The thermodynamic parameters resulting from the DSC study are summarized in Table I. Table I indicates that PP and its nanocomposites seemed to have almost the same value of T_m. On the basis of the area of the heating curves shown in Figure 6, the degree of crystallinity (X_c) values of PP and its nanocomposites were calculated with the following equation:[22]

$$X_c = \frac{\Delta H}{(1-j)\Delta H_0} \times 100\%$$

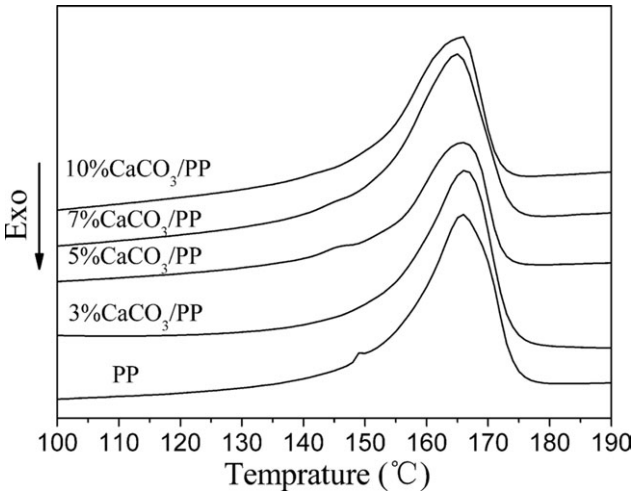

Figure 6. DSC melting curves of the original PP and PP/5% nano-$CaCO_3$ composites. The heating rate was 20°C/min.

Table I. T_m, ΔH, and X_c Values of the PP and the Nanocomposites

Sample	ΔH (J/g^{-1})	T_m (°C)	X_c (%)
PP	100.08	165.94	47.89
PP/3% nano-$CaCO_3$	91.59	166.70	45.18
PP/5% nano-$CaCO_3$	91.64	166.37	46.15
PP/7% nano-$CaCO_3$	90.33	165.23	46.47
PP/10% nano-$CaCO_3$	87.30	166.59	46.41

ΔH, heat of fusion.

where ΔH is the endothermic enthalpy of the sample, ΔH_0 is the endothermic enthalpy of PP when it crystallizes completely (the value was set as 209.0 J/g), and j is the mass fraction of the filler. X_c for the nanocomposites was lower than that of PP. Lin et al.[27] also found the decrease in crystallinity in PP/modified nano-$CaCO_3$, which they attributed to the coating of modifiers on the nano-$CaCO_3$.

Effect of the Nano-$CaCO_3$ Content

Figure 7 displays the SEM micrographs of the PP and its nanocomposite foams. Figure 8 quantitatively shows the average cell diameter and cell density distributions for the PP and its nanocomposite foams. In comparison with PP, the nanocomposites exhibited dramatically improved foamability and showed significantly improved cell structures and properties, including the cell diameter and the cell density. They had an average cell diameter in the range of 6.2–12.1 μm, which was smaller than that observed for the PP foam. Many other researchers have reported that blending nanoparticles into PP can improve the foamability.[6,17,27]

It can be seen from Figure 8 that the cell diameter increased and the cell density decreased, both in a nearly linear manner, with increasing nano-$CaCO_3$ content up to 5 wt %. A further increase in the nano-$CaCO_3$ content to 10 wt % led to a sharp increase in the cell diameter and a significant decrease in the cell density. The nanoparticles had large surface areas and could serve as heterogeneous nucleation sites at which embryos are formed at lower free energy during the foaming of the nanocomposites. In this study, the presence of the nano-$CaCO_3$ led to an increase in the nucleation rate; this increased the cell density and decreased the cell diameter. However, when too much nano-$CaCO_3$ was blended into PP, the nano-$CaCO_3$ aggregated, and the surface area and heterogeneous sites decreased; this led to larger cells and a lower cell density.

Effect of the Foaming Temperature

Figure 9 shows the variations of the cell diameter, cell density, and foam density with the foaming temperature for PP and its nanocomposite foams. We found that with increasing temperature, the PP foams showed an apparent increase in cell size, whereas the nanocomposite foams first exhibited an apparent increase in the cell size versus the foaming temperature and then varied very slightly. In the case of the temperature dependence of the cell density, a significant decrease was observed, and then, the change was much lower for the PP foams, whereas the nanocomposite foams had the same tendency but more apparently. This behavior was due to the slight decrease in SC-CO_2

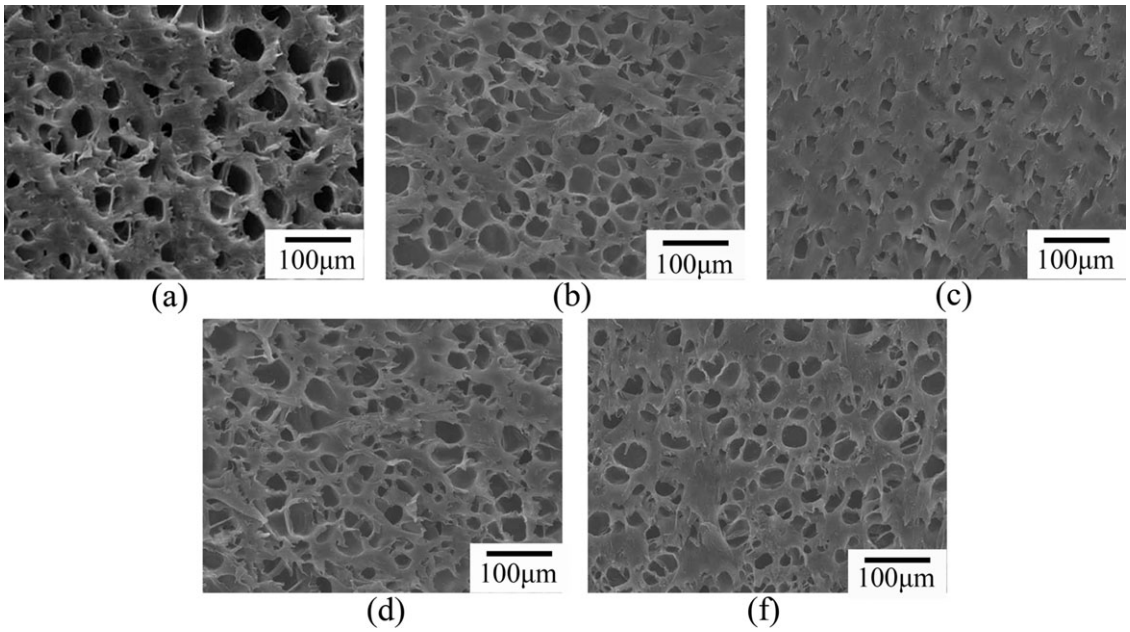

Figure 7. SEM micrographs of the original PP and PP/5% nano-$CaCO_3$ foams at a foaming temperature of 150°C, an infiltration temperature of 80°C, a saturation pressure of 25 MPa, and a foaming time of 10 min. The contents of the nano-$CaCO_3$ were (a) 0, (b) 3, (c) 5, (d) 7, and (e) 10 wt %.

dissolved in the matrix for PP and the action of the heterogeneous sites (nano-$CaCO_3$) in cell nucleation for nanocomposites as the prominent factor decreasing the foaming temperature. Both the cell density and cell size affected the foam density. Here, the foam density decreased with increasing temperature from 150 to 152°C and then remained almost constant. From the previous results, we can say that the behavior of foam density was mainly due to the competition between cell nucleation and cell growth. Cell growth played a dominant role in the determination of the foam density at low temperatures (from 150 to 152°C). Although the cells grew slightly, the foam density decreased dramatically. However, at high temperatures, both the cell diameter and cell density hardly influenced the foam density. This may have been because the solubility of CO_2 remained almost constant with increasing temperature at high temperatures. These phenomena were a little different from Nam's achievements.[7]

As shown in Figure 10, an interesting phenomenon was observed. For the PP foams, small and large cells were apparent at the low (152°C) and high (158°C) temperatures, but at the moderate temperature (154°C), all of the cells were uniform. For the nanocomposite foams, this phenomenon was not observed. The mechanisms of the similar phenomena at low and high temperatures were different. At low temperature, this may have been due to the influence of the crystalline regions. It has been reported that when the depressurization rate was high enough at low temperature, cell nucleation in the crystalline region became possible.[3] Once cell nuclei were formed, more CO_2 molecules were inclined to diffuse into them instead of generating new cell nuclei. Moreover, the amorphous region was much less rigid than the crystalline region. Thus, cells in the amorphous region grew bigger and bigger in size than those in the crystalline region. At a temperature of 154°C, most of the crystalline regions were disrupted, and there was no difference

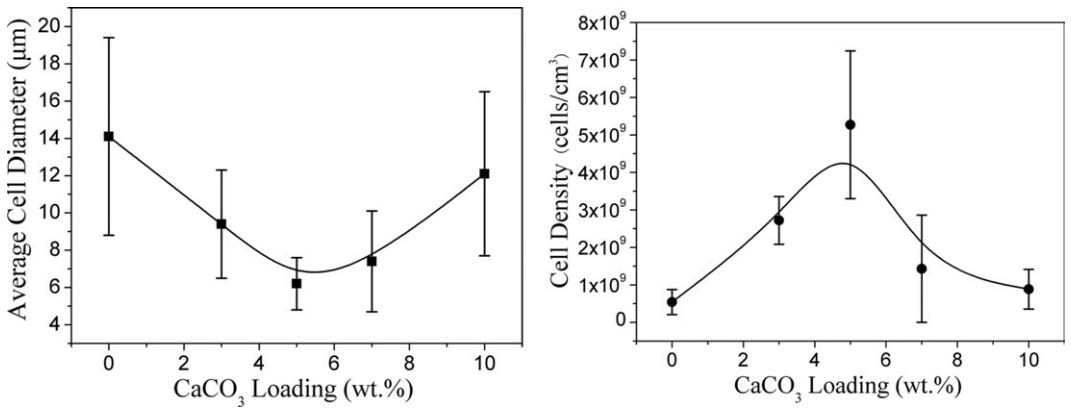

Figure 8. Average cell diameter and cell density of the original PP and PP/5% nano-$CaCO_3$ foams as influenced by the nano-$CaCO_3$ loading.

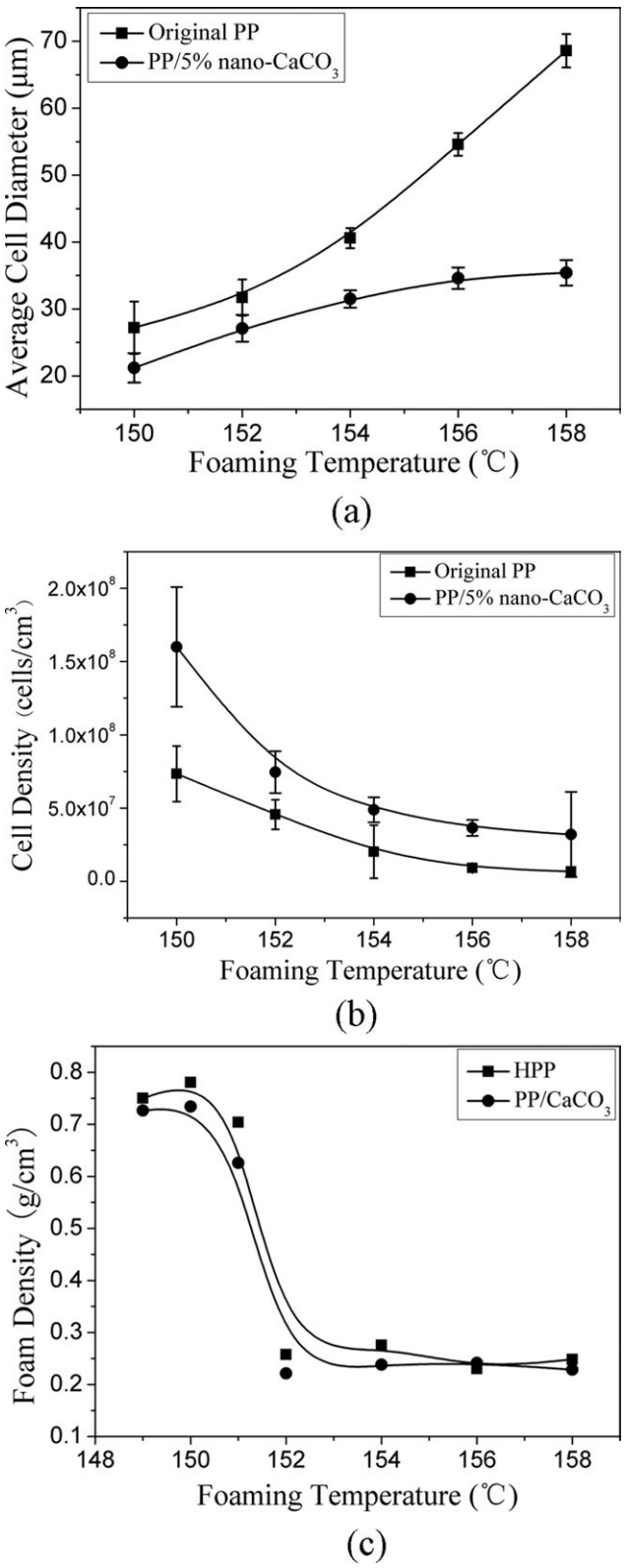

Figure 9. Average cell diameter, cell density, and foam density of the original PP and PP/5% nano-$CaCO_3$ foams as influenced by the foaming temperature. The infiltration temperature was 80°C, the saturation pressure was 25 MPa, and the foaming time was 30 min.

between crystalline and amorphous regions, so all of the cells were uniform. At high temperature, cell coalescence led to irregular cells. However, in the nanocomposites, the nucleation effect and the decrease in crystallinity reduced the difference between the crystalline and amorphous regions, and all of the cells were uniform.

Effect of the Saturation Pressure

Figure 11 shows that the cell diameter and cell density of the PP and its nanocomposite foams varied with the saturation pressure. The pressure ranged from 20 to 28 MPa. At the lowest pressure of 20 MPa, the cell diameter and cell density of the PP and its nanocomposite foams were very low. When the pressure increased from 22 to 28 MPa, the cell diameter of PP decreased, and the cell density increased. However, the nanocomposite foams exhibited a constant cell diameter and density versus saturation pressure. When the saturation pressure was very low, the extent of the CO_2-induced T_m depression was low and so was the amount of CO_2 dissolved in PP and its nanocomposites. Thus, PP and its nanocomposite foams were stiff, and their deformability and foamability were limited. Figure 12(a,b) shows the SEM micrographs of the PP and its nanocomposite foams at a pressure of 20 MPa. As indicated in these micrographs, only a small amount of discrete cells were formed on the samples, and large unfoamed regions were apparent.

When the pressure ranged from 22 to 28 MPa, both the amount of CO_2 dissolved in PP and the CO_2-induced T_m depression were higher than those at 20 MPa; the samples became soft enough, and the cells were nucleated and expanded easily. Thus, a higher pressure led to more cells being nucleated within a given volume, which led to smaller cells and a higher cell density for the PP foams. Although the constant cell diameter and cell density for the nanocomposite foams was due to the heterogeneous effect of nano-$CaCO_3$, nano-$CaCO_3$, as a kind of heterogeneous site, benefited nucleation, but it could also inhibit gas expansion and cell growth. Figure 12(c,d) shows the SEM micrographs of the PP and its nanocomposite foams at a pressure of 22 MPa. It can be seen that the foamability of PP and its nanocomposites improved dramatically because there were no large unfoamed regions observed in the samples.

Effect of the Infiltration Temperature

The effect of the infiltration temperature on the cell morphology of PP and its nanocomposite foams was studied at a foaming temperature of 154°C, a saturation pressure of 25 MPa, and a foaming time of 30 min. Figure 13 shows that a lower infiltration temperature led to larger cells and a lower cell density. This was because a lower infiltration temperature decreased the *initial foaming temperature* ($T_{initial}$), which was the temperature at which samples were apparently foamed. Figure 14 shows the foam density variation with the foaming temperature at different infiltration temperatures. $T_{initial}$ decreased with decreasing infiltration temperature. Although at an infiltration temperature of 80°C, the samples foamed at 150°C, we refer $T_{initial}$ to 151°C, because the foam density did not decline dramatically; this means that the samples were only partially foamed, not apparently foamed. The reasons for this partial foaming is evidenced in the next section.

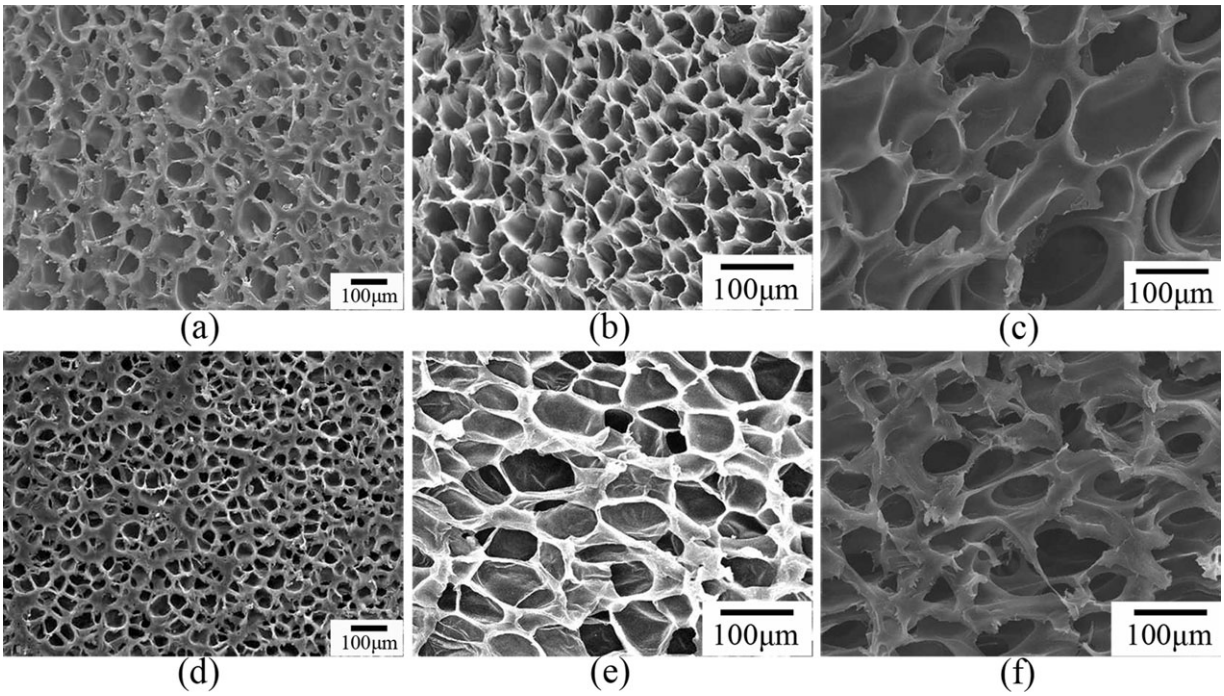

Figure 10. SEM micrographs of the original PP and PP/5% nano-$CaCO_3$ foams at different foaming temperatures at a saturation pressure of 25 MPa, an infiltration temperature of 80°C, and a foaming time of 30 min. The foams were (a–c) the original PP foams and (d–f) the PP/5% nano-$CaCO_3$ foams. The foaming temperatures were (a,d) 152, (b,e) 154, and (c,f) 158°C.

In Figure 15, it can be seen that the cell walls became thinner with decreasing infiltration temperature and were finally disrupted at an infiltration temperature of 40°C. The cells coalesced, which was the reason why the cell diameter increased dramatically with decreasing infiltration temperature at a low infiltration temperature.

Effect of the Foaming Time

With the method described in Figure 1(a), cells could form at the increasing temperature or depressurization stage. To determine at which stage cells were formed, an experiment was conducted as follows: PP and its nanocomposites were dipped at 25 MPa and 80°C for 24 h. Then, the temperature was raised to 154°C within 20 min and kept there for 30 min. The system was cooled to room temperature without a change in pressure, and the vessel was depressurized to atmospheric pressure. Finally, the samples were injected out and examined with SEM. No cells were observed. However, as shown in Figure 10(b,e), when the samples were foamed in the same foaming conditions with the process described in Figure 1(a), lots of cells were formed; this indicated that cells were formed in the depressurization stage.

When the infiltration temperature increased to the foaming temperature, it took some time to transfer heat from the surface to the interior. When the time was very short, the surface and

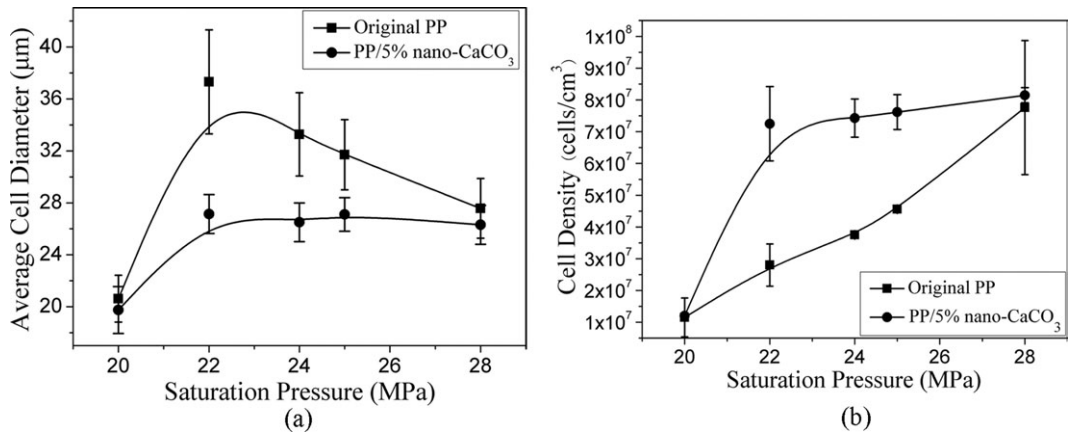

Figure 11. Average cell diameter and cell density of the original PP and PP/5% nano-$CaCO_3$ foams as influenced by the saturation pressure. The foaming temperature was 152°C, the infiltration temperature was 80°C, and the foaming time was 30 min.

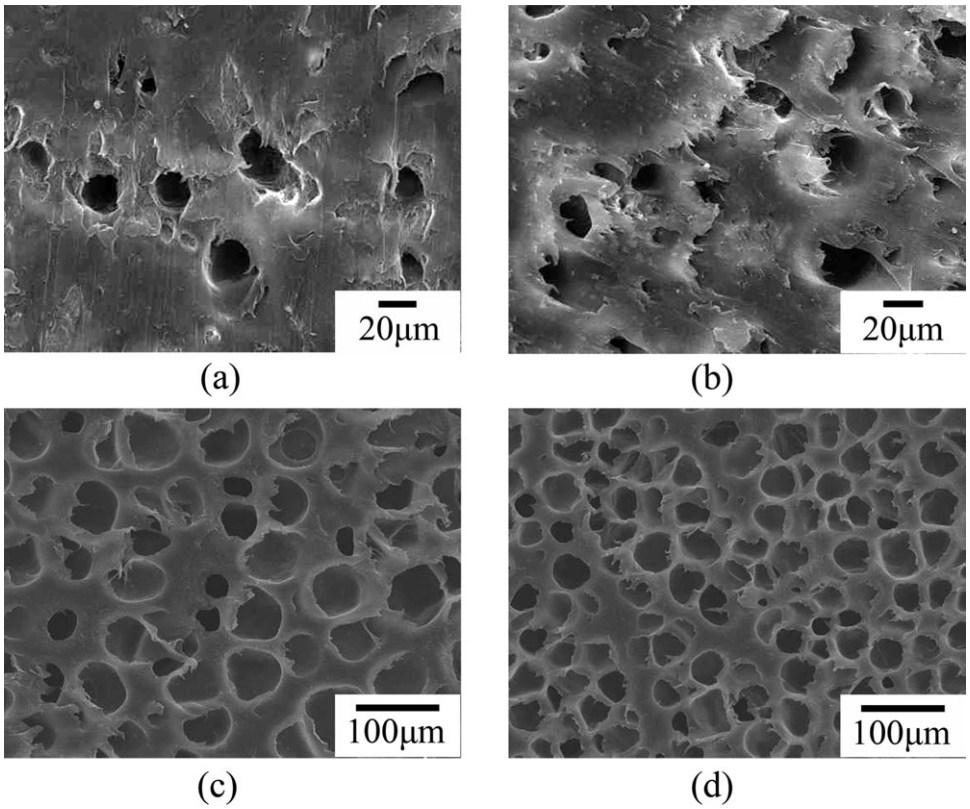

Figure 12. SEM micrographs of the original PP and PP/5% nano-$CaCO_3$ foams at different saturation pressures at a foaming temperature of 152°C, an infiltration temperature of 80°C, and a foaming time of 30 min. The foams were the (a,b) original PP and (c,d) PP/5% nano-$CaCO_3$ foams. The pressures were (a,c) 20 and (b,d) 22 MPa.

interior of the polymer were soft and intact, respectively. The surface was more advantageous for cell growth. Therefore, cells were different between the surface and interior. Figure 16(a) shows the SEM micrographs of the cell structure of PP when the foaming time was only 10 min. As shown in Figure 16(a), a decrease in the cell diameter from the surface to the interior of PP was apparent. We refer this structure as the *skin–core structure*. When the foaming time was prolonged to 45 min, the cellular structures of the surface and interior became similar, as shown in Figure 16(b). The cellular structure hardly changed when the foaming time ranged from 45 to 60 min. This was because the polymer became completely soft when the foaming time was 45 min. A longer foaming time hardly caused any change, so the samples were partially foamed at 30 min. Figure 17 shows the variations in the cell diameter and cell density with foaming time. We observed that the cell diameter

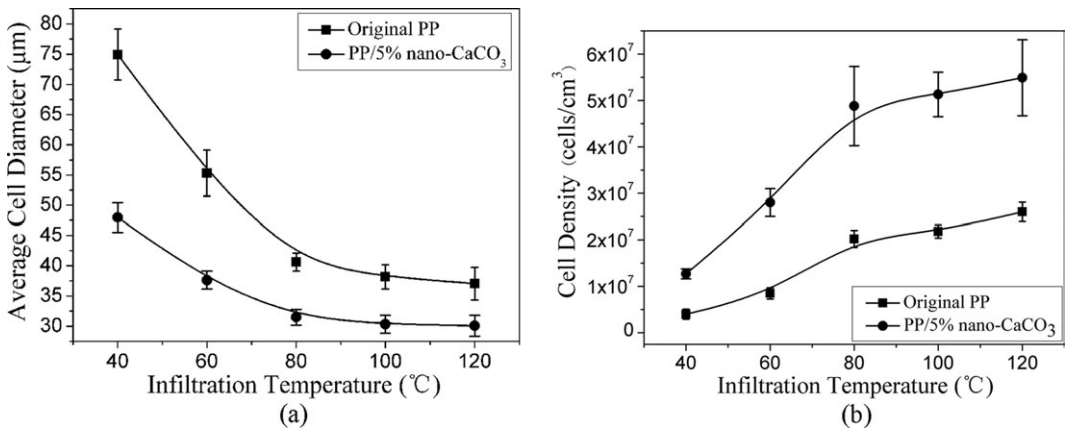

Figure 13. Average cell diameter and cell density of the original PP and PP/5% nano-$CaCO_3$ foams as influenced by the infiltration temperature. The foaming temperature was 154°C, the saturation temperature was 25 MPa, and the foaming time was 30 min.

Applied Polymer SCIENCE

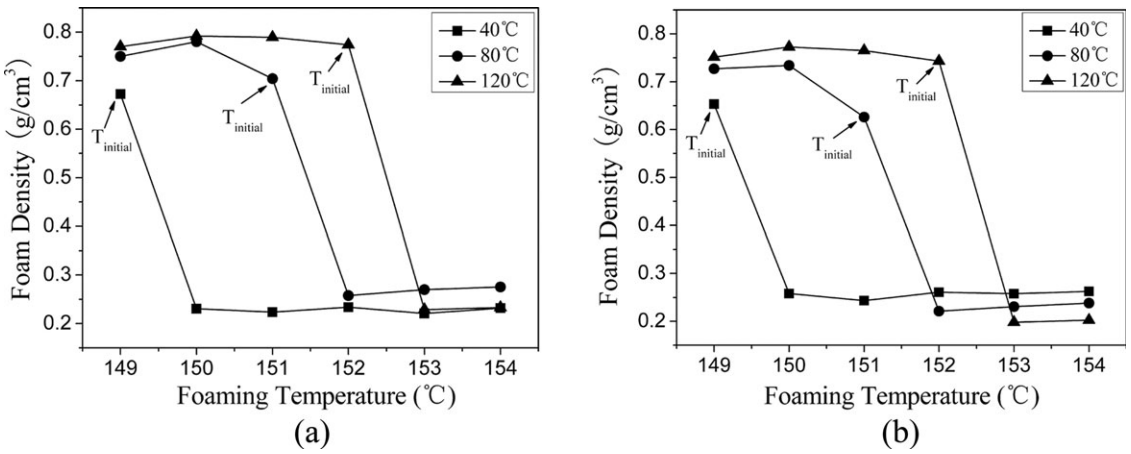

Figure 14. Foam density variation with the foaming temperature at different infiltration temperatures. The samples were (a) the original PP and (b) the PP/5% nano-$CaCO_3$.

decreased and the cell density increased apparently when the foaming time was increased from 10 to 45 min but hardly any change was observed from 45 to 60 min.

Orthogonal Experimental Design

Orthogonal experimental design is a mathematical method used for planning multifactor tests. In this case, we used this method to further explore the effects of the previous five factors. Each of the previous five factors could be changed at four levels, and an $L_{16}(4^5)$ orthogonal array was used to arrange the tests. The effects of each of these five factors on the expansion ratio and cell diameter were then examined. Details of the four levels for each factor are shown in Table II. Equations (2) and (3) show that both the expansion ratio and cell diameter influenced the cell density. The cell diameter and cell density are very important parameters in characterizing cell morphologies. Therefore, in this study, we investigated the influence of various factors on the expansion ratio and cell diameter.

Sixteen experiments in accordance with the $L_{16}(4^5)$ orthogonal array were performed. The results of the effects of the five factors on the cell diameter are presented in Table III. As shown, K_{1j} and M_{1j} represent the sum of the results of row j when the level was 1. K_j and M_j represent the difference in the largest and smallest K_{ij} and M_{ij} values of row j. A large value of K_j or M_j indicates that the effect of factor j on the expansion ratio or cell diameter was significant. Meanwhile, K and M correspond to the sums of the total results. From the K_j values in Table III, one can see that $4.99 > 4.55 > 4.03 > 2.84 > 2.82$. The effects of the five factors on the expansion ratio can consequently be

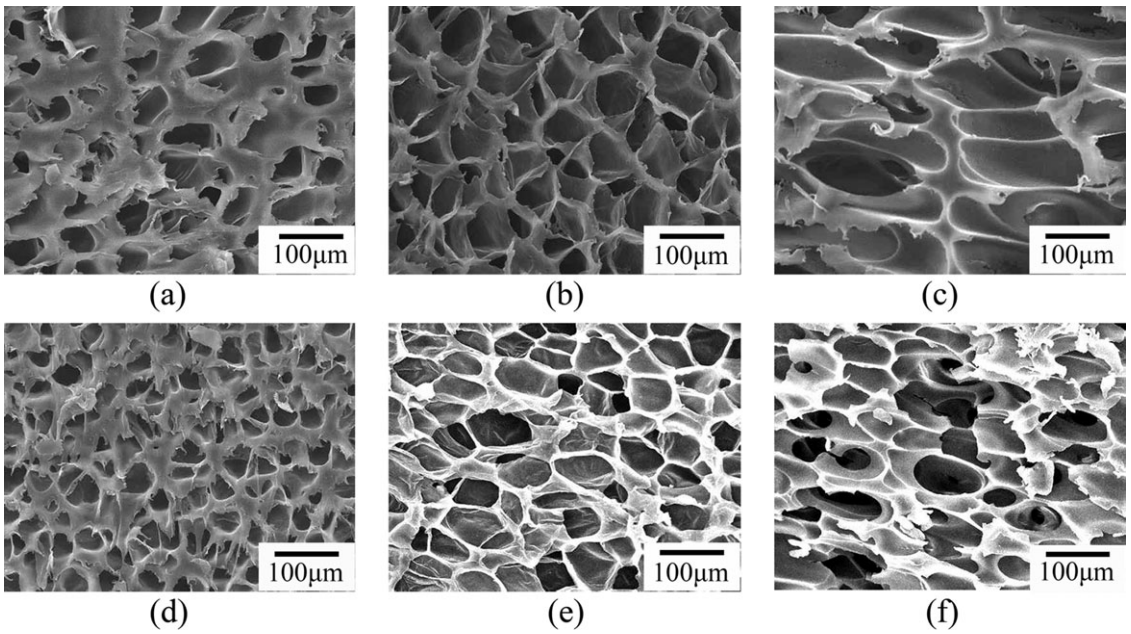

Figure 15. Cell structures at different infiltration temperatures at a foaming temperature of 154°C, a saturation pressure of 25 MPa, and a foaming time of 30 min. The foams were (a–c) the original PP foams and (d–f) PP/5% nano-$CaCO_3$ foams. The infiltration temperatures were (a,d) 120, (b,e) 80, and (c,f) 40°C.

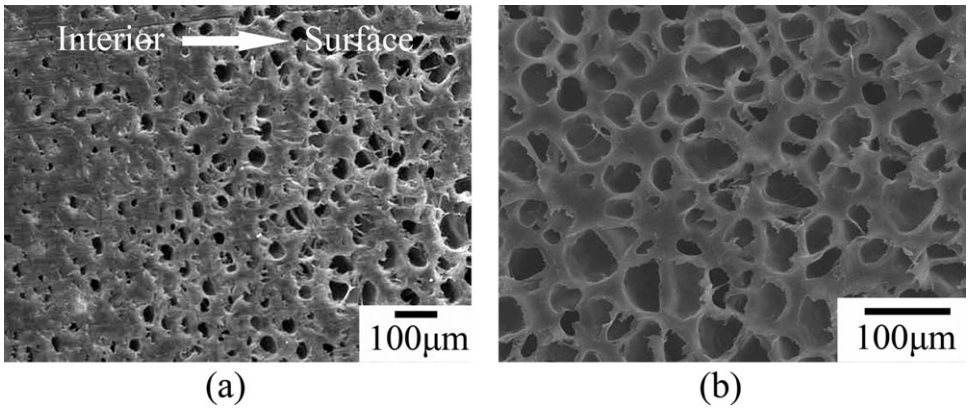

Figure 16. SEM micrographs of the original PP foams at different foaming times and at a foaming temperature of 150°C, a saturation pressure of 25 MPa, and an infiltration temperature of 80°C. The foaming times were (a) 10 and (b) 45 min.

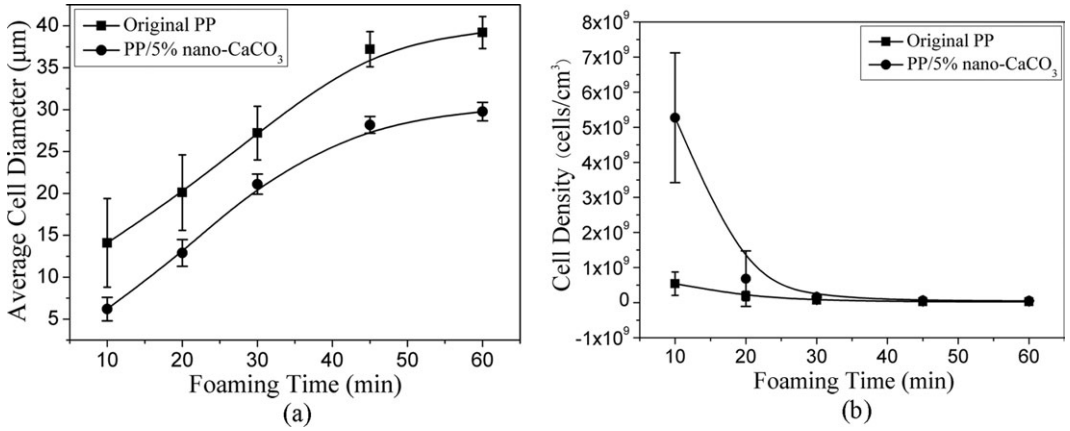

Figure 17. Average cell diameter and cell density values of the original PP and PP/5% nano-$CaCO_3$ foams as influenced by the foaming time. The foaming temperature was 150°C, the saturation pressure was 25 MPa, and the infiltration temperature was 80°C.

listed in the following order: Saturation pressure > Infiltration temperature > Nano-$CaCO_3$ loading > Foaming temperature > Foaming time. From the M_j values, 108.33 > 69.34 > 58.36 > 56.04 > 41.06, the effect of the five factors on the cell diameter can consequently be listed in the following order: Foaming temperature > Saturation pressure > Infiltration temperature > Nano-$CaCO_3$ loading > Foaming time.

From previous results, we observed that the foaming temperature influenced the cell diameter significantly, but its effect on the expansion ratio was very weak because of the apparent increase in the gas diffusion rate and the slight decrease in the amount of SC-CO_2 dissolved in the PP matrix with increasing foaming temperature. The saturation pressure was an important factor influencing the cell diameter and expansion ratio; this was caused by the increasing solubility of SC-CO_2 with increasing pressure. Therefore, it is an effective method for obtaining microcellular foams through variation of the saturation pressure. The infiltration temperature significantly influenced the expansion ratio and cell diameters of PP and its nanocomposites. Its effect on the expansion ratio and cell diameter was even more significant than that of nano-$CaCO_3$ loading. Nano-$CaCO_3$ loading dramatically decreased the cell diameters of the

Table II. Contents of Orthogonal Factors and Levels

Factor level	A: Foaming temperature (°C)	B: Saturation pressure (MPa)	C: Infiltration temperature (°C)	D: Foaming time (min)	E: Nano-$CaCO_3$ loading (%)
1	152	20	40	10	0
2	154	22	60	20	3
3	156	25	80	30	5
4	158	28	120	60	10

Table III. Effect of the Five Factors on the Cell Diameter

Experiment	A: Foaming temperature (°C)	B: Saturation pressure (MPa)	C: Infiltration temperature (°C)	D: Foaming time (min)	E: Nano-$CaCO_3$ loading (%)	Expansion ratio	Average cell diameter (μm)
1	1	1	1	1	1	1.43	28.35
2	1	2	2	2	2	3.55	31.30
3	1	3	3	3	3	4.51	27.10
4	1	4	4	4	4	4.42	32.62
5	2	1	2	3	4	3.42	40.16
6	2	2	1	4	3	4.12	38.95
7	2	3	4	1	2	3.98	34.58
8	2	4	3	2	1	5.23	30.32
9	3	1	3	4	2	4.11	45.22
10	3	2	4	3	1	3.50	87.15
11	3	3	1	2	4	3.72	48.99
12	3	4	2	1	3	4.36	40.30
13	4	1	4	2	3	4.31	60.35
14	4	2	3	1	4	4.22	57.34
15	4	3	2	4	1	3.11	67.85
16	4	4	1	3	2	4.25	42.16
K_{1j}	13.91	13.27	13.52	13.99	13.27	$K = 61.76$	
K_{2j}	16.75	15.39	14.44	16.81	15.89		
K_{3j}	15.29	15.32	18.07	15.68	17.30		
K_{4j}	15.81	18.26	16.21	15.76	15.78		
K_j	2.84	4.99	4.55	2.82	4.03		
M_{1j}	119.37	174.08	158.45	160.57	213.67		$M = 712.74$
M_{2j}	144.01	214.74	179.61	170.96	157.63		
M_{3j}	221.66	174.62	216.81	201.63	176.74		
M_{4j}	227.70	145.40	214.70	184.64	179.11		
M_j	108.33	69.34	58.36	41.06	56.04		

nanocomposites compared with those of the original PP foams. However, the cell diameters of the nanocomposites containing 3, 5, and 10% nano-$CaCO_3$ varied very slightly with the nano-$CaCO_3$ loading.

Comparison to the Conventional Process

It has been reported that the foaming temperature range of PP with the conventional process described in Figure 1(b) was very narrow; this makes it difficult for PP to foam, and the cell

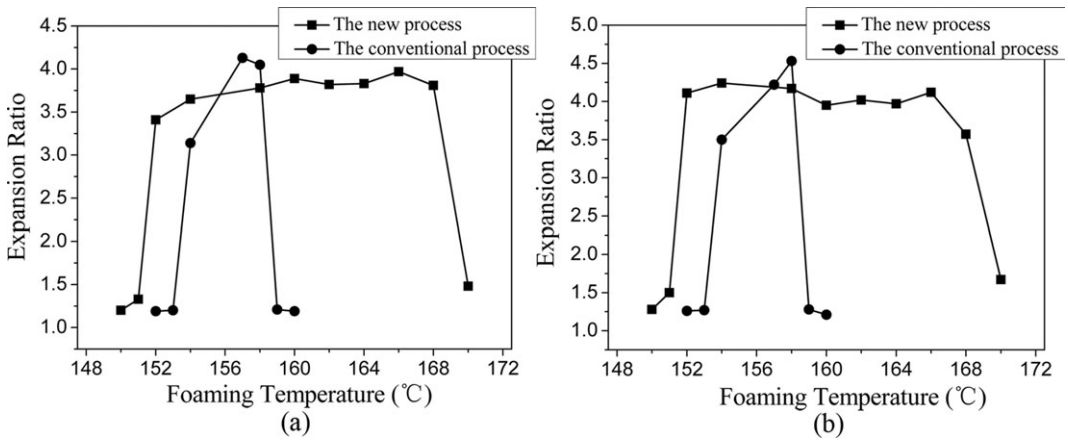

Figure 18. Expansion ratios of the original PP and PP/5% nano-$CaCO_3$ foams with the foaming temperature with different processes. The saturation pressure was 25 MPa, the foaming time was 30 min, and the infiltration temperature was 80°C. The foams were (a) the original PP and (b) PP/5% nano-$CaCO_3$ foams.

morphologies difficult to control. Therefore, the narrow foaming temperature range has become one of the critical obstructions to the foaming of PP.

Figure 18 shows the variations of the expansion ratio with the foaming temperature in two processes: one is the new process described in Figure 1(a), and the other is the conventional one described in Figure 1(b). As shown in Figure 18, the foaming temperature range of the new process was about five times broader than that of the conventional one; this improved upon the difficulties in the foaming of PP. This might have been due to the plasticization effect of SC-CO_2 for PP in the infiltration stage. The plasticization effect increased the ability of PP to resist temperature variation. However, this must be investigated further.

CONCLUSIONS

In this work, we systematically studied a new foaming process and compared it with the conventional one. The experimental results reveal that the nanocomposites largely had decreased cell diameters and, hence, increased cell density compared to the PP foams. The cellular structures of the PP foams were more sensitive to the foaming temperature and saturation pressure variations than those of the nanocomposites. Uniform cells were only observed at the moderate temperature for PP, whereas the cells of the nanocomposites were always uniform. The foam density was dependent on the competition between cell growth and cell nucleation. At a very low saturation pressure, the cell density was low, and the cell diameter was small because of the low CO_2-induced T_m depression. A lower infiltration temperature decreased $T_{initial}$ and thus led to larger cells and a lower cell density. The foaming time influenced the heat transfer from the surface to the interior of the polymer. Therefore, a short foaming time led to a skin–core structure, but when the foaming time was increased, the skin–core structure disappeared, the cell diameter increased, and the cell density decreased. When the foaming time was greater than 45 min, the cell structures were hardly changed. From the results of the orthogonal experiments, we determined that the infiltration temperature was a significant factor affecting the cell diameter. Compared with the conventional process, the new process had a much broader foaming temperature range.

REFERENCES

1. Rachtanapun, P.; Selke, S. E. M.; Matuana, L. M. *J. Appl. Polym. Sci.* **2003,** *88*, 2842.
2. Siripurapu, S.; Gay, Y. J.; Royer, J. R. *Polymer* **2002,** *43*, 5511.
3. Xu, Z. M.; Jiang, X. L.; Liu, T. *J. Supercrit. Fluids* **2007,** *41*, 302.
4. Liu, H.; Chuai, C. Z.; Iqbal, M. *J. Appl. Polym. Sci.* **2011,** *122*, 973.
5. Naguib, H. E.; Park, C. B.; Reichelt, N. *J. Appl. Polym. Sci.* **2004,** *91*, 2661.
6. Huang, H. X.; Wang, J. K. *J. Appl. Polym. Sci.* **2007,** *106*, 506.
7. Nam, P. H.; Maiti, P.; Okamoto, M.; Kotaka, T. *Polym. Eng. Sci.* **2002,** *42*, 1909.
8. Pötschke, P.; Krause, B.; Stange, J.; Münstedt, H. *Macromol. Symp.* **2007,** *254*, 407.
9. Goren, K.; Chen, L. *J. Supercrit. Fluids* **2010,** *51*, 420.
10. Li, D. C.; Liu, T.; Zhao, L.; Yuan, W. K. *Ind. Eng. Chem. Res.* **2009,** *48*, 7121.
11. Lei, Z. G.; Ohyabu, H.; Sato, Y.; Inomata, H. *J. Supercrit. Fluids* **2007,** *40*, 456.
12. Wang, J.; Cheng, X. G.; Yuan, M. J.; He, J. S. *Polymer* **2001,** *42*, 8267.
13. Rachtanapun, P.; Selke, S. E. M.; Matuana, L. M. *J. Appl. Polym. Sci.* **2003,** *88*, 2483.
14. Huang, H.; Bing, H.; Wang, L. *J. Appl. Polym. Sci.* **2011,** *119*, 1527.
15. Lin, Y.; Chen, H. B.; Chan, C. M. *J. Colloid Interface Sci.* **2011,** *354*, 576.
16. Lipinska, M.; Zaborki, M.; Slusarski, L. *Macromol. Symp.* **2003,** *194*, 294.
17. Zhu, B.; Zha, W. B.; Yang, J. T.; Zhang, C. L. *Polymer* **2010,** *51*, 2178.
18. Tran, H. V.; Tran, L. D.; Vu, H. D. *Colloids Surf. A* **2010,** *366*, 100.
19. Lam, T. D.; Hoang, T. V.; Quang, D. T.; Kim, J. S. *Mater. Sci. Eng. A* **2009,** *501*, 89.
20. Huang, H. X.; Xu, F. H. *Polym. Adv. Technol.* **2011,** *22*, 822.
21. Kiss, A.; Fekete, E.; Pukánszky, B. *Compos. Sci. Technol.* **2007,** *67*, 157.
22. Wan, W. T.; Yu, D. M.; Xie, Y. C. *J. Appl. Polym. Sci.* **2006,** *102*, 3484.
23. Li, L.; Liu, T.; Zhao, L.; Yuan, W. K. *J. Supercrit. Fluids* **2011,** *60*, 137.
24. Zare, Y.; Garmabi, H. *J. Appl. Polym. Sci.* **2012,** *124*, 1229.
25. Chen, H. B.; Wang, M. Z.; Lin, Y.; Chan, C. M.; Wu, J. S. *J. Appl. Polym. Sci.* **2007,** *106*, 3413.
26. Chiu, F. C.; Lai, S. M.; Wong, C. M.; Chang, C. H. *J. Appl. Polym. Sci.* **2006,** *102*, 2280.
27. Lin, Z. D.; Huang, Z. Z.; Zhang, Y.; Mai, K. C.; Zeng, H. M. *J. Appl. Polym. Sci.* **2004,** *91*, 2452.